Two-Dimensional Analysis Photothermal Properties in Nanoscale Plasmonic Waveguides for Optical Interconnect

Qiang Li, *Member, IEEE*, Weichun Zhang, Hang Zhao, and Min Qiu, *Senior Member, IEEE*

***Abstract*—The inevitable light absorption in plasmonic waveguides (PWs) gives rise to heating of waveguides themselves. Here the photothermal effects in nanowire PWs, slot PWs, channel PWs, dielectric-loaded PWs and hybrid PWs are investigated in the cross section. The resistive heating is significant for all waveguides. The thermal feature sizes of the PWs are the main factors limiting the integration density. The copper PWs show the largest temperature rise compared with the gold PWs, the silver PWs and the aluminum PWs. These findings unveil the physical properties of PWs from the photothermal perspective and provide insights into the underlying factors influencing the adoption of PWs in optical interconnect.**

***Index Terms*—Optical interconnect, photothermal effect, plasmonic.**

I. Introduction

As the dominating electronic devices are approaching an interconnect bottleneck owing to the increased signal delay and the high thermal dissipation, photonic devices may offer new solutions because of their high bandwidth and reduced power dissipation [1]–[4]. However, the sizes of photonic devices are ultimately diffraction limited. For example, the critical dimension of silicon photonic structure is around 500 nm. For electronic structure, this critical dimension can be shrunk to below 50 nm. Therefore, photonic structures tend to be at least one order of magnitude larger than their electronic counterparts [1]–[4]. The surface plasmon polaritons (SPPs), which are optically induced coherent oscillations of free electrons at metal/dielectric interfaces, can spatially allow the concentration of light well beyond the diffraction limit. Owing to this unique property, the SPP technology provides a potential solution in future high-capacity integrated circuit [1]–[4]. Thus far, several strategies for guiding SPPs have been demonstrated for integration circuits [1], including metallic nanowire plasmonic waveguides (PWs) [5], metal–insulator–metal slot PWs [6]–[8], channel PWs [9], dielectric-loaded PWs [10], hybrid PWs [11], etc.

When the light is guided through any plasmonic structure, the inevitable absorption by metal is ultimately converted to heat [12]–[25]. The generated heat can be utilized in a set of applications such as photothermal cancer therapy [14], materials science [15], optical data storage [16], nanofluidics [17], nanotweezers [18], photonic switch [19], and plasmon ruler [20], etc. For PWs, while most of the research has focused on the optical properties for high-density plasmonic integration, their photothermal properties which have a side effect on the optical interconnect are still yet to be explored. Whether the maximum integration density for plasmonic devices in optical interconnect is restricted by its optical or thermal feature size just as the electronic devices is still unexplored. Therefore, it is of vital importance to unveil the photothermal properties in PWs.

To address this issue, we investigate the photothermal properties in PWs in this paper. Five typical kinds of PWs are taken into consideration: (1) nanowire PW, (2) slot PW, (3) channel PW, (4) dielectric-loaded PW and (5) hybrid PW. Four metals are considered: gold, silver, copper and aluminum. Gold and silver are noble metals conventionally adopted as the plasmonic materials. Copper and aluminum are alternate metals compatible with the main stream CMOS fabrication. The remainder of the paper is organized as follows. Section II describes the five plasmonic structures and simulation method briefly. Section III investigates the optical properties of the PWs, including the mode distribution and the resistive loss. Section IV investigates the thermal properties of the PWs, including spatial thermal properties, and maximum temperature rise versus waveguide geometries and metal materials. Finally, the conclusions are drawn in Section V.

II. Structure and Simulations

Five typical kinds of PWs that can be used in optical interconnect are considered in this paper and their schematic diagrams are depicted in Fig. 1(a): (1) nanowire PW, which is formed by immersing a metal nanowire in a SiO_2 matrix; (2) slot PW,

Manuscript received June 30, 2013; revised September 19, 2013; accepted September 27, 2013. Date of publication October 27, 2013; date of current version November 27, 2013. This work was supported in part by the National Natural Science Foundation of China under Grants 61275030, 61205030, and 61235007, in part by the Qianjiang River Fellow Fund of Zhejiang Province, in part by the Opened Fund of State Key Laboratory of Advanced Optical Communication Systems and Networks, in part by the Fundamental Research Funds for the Central Universities, in part by the Doctoral Fund of Ministry of Education of China under Grant 20120101120128, in part by the Scientific Research Foundation for the Returned Overseas Chinese Scholars from the State Education Ministry, in part by the Swedish Foundation for Strategic Research (SSF), and in part by the Swedish Research Council (VR).

Q. Li, W. Zhang, and H. Zhao are with the State Key Laboratory of Modern Optical Instrumentation, Department of Optical Engineering, Zhejiang University, Hangzhou 310027, China (e-mail: qiangli@zju.edu.cn; zhwc@zju.edu.cn; zhaohang0124@gmail.com).

M. Qiu is with the State Key Laboratory of Modern Optical Instrumentation, Department of Optical Engineering, Zhejiang University, Hangzhou 310027, China and also with the School of Information and Communication Technology, KTH Royal Institute of Technology, Electrum 229, 16440 Kista, Sweden (e-mail: minqiu@zju.edu.cn).

Color versions of one or more of the figures in this paper are available online at http://ieeexplore.ieee.org.

Digital Object Identifier 10.1109/JLT.2013.2284237

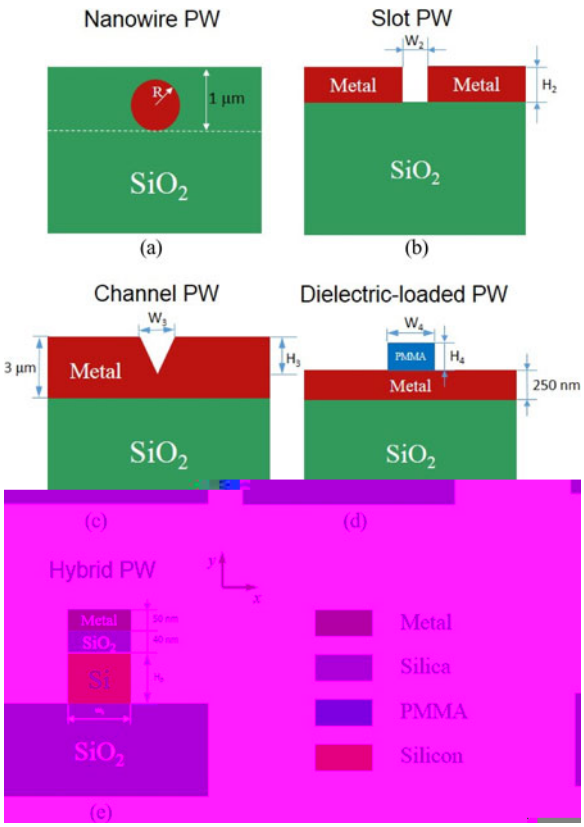

Fig. 1. Schematic diagram of the PWs. (a) Nanowire PW, (b) slot PW, (c) channel PW, (d) dielectric-loaded PW, and (e) hybrid PW.

where an air trench is etched through the metal film; (3) channel PW, in which a V-shaped air groove is milled in a metal film; (4) dielectric-loaded PW, which is formed by depositing a PMMA ridge on a metal surface; (5) hybrid PW, consisting of a metal cap separated from a high-permittivity Si ridge by a nanoscale SiO_2 gap.

A. Mode Simulation

The mode analysis is performed in the cross-section plane ($x-y$ plane) of the PW. The surface plasmon wave propagates in the z direction and the electric field varies as $e^{(i\beta z - i\omega t)}$, where ω is the angular frequency and β is the complex propagation constant. β is related to the effective mode index n_{eff} by $\beta = 2\pi n_{\text{eff}}/\lambda$. The magnetic field H profile in the cross-section plane is governed by the Helmholtz equation:

$$\nabla \times \left(\frac{1}{\nabla n^2}\nabla \times \mathbf{H}\right) - k_0^2 \mathbf{H} = 0 \tag{1}$$

where n denotes the material refractive index (provided in Table I). The propagation length of the plasmon mode is defined as $L = 1/2\ \text{Im}\{\beta\}$. The light wavelength is assumed to be at telecommunication wavelength 1550 nm. The strong photothermal effect could lead to the change in the refractive index of a dielectric material but shows little impact on the refractive index of metal. Since the heat source dominating the heat transfer is mainly related to the metal loss, thermo-optic effect of the dielectric on the thermal behavior is thus not considered here and the refractive indices are assumed to be constants.

TABLE I
MATERIAL PARAMETERS USED FOR SIMULATION

	Permittivity ε	Thermal conductivity k (W/(m·K))
Au	-95.9236+10.9676i	317.72
Ag	-86.6424+8.7422i	428.77
Cu	-67.86+10.0111i	386.6
Al	-242.62+49.417i	236.1
SiO_2	2.1025	1.3672
Si	12.25	152.46
PMMA	2.2261	0.2

The permittivities for Au/Ag/Cu are from Ref. [26]. The permittivity for Al is from Ref. [27]. The thermal conductivities for metal, SiO_2 and Si are from the Comsol Material library. The parameters for PMMA are from Ref. [28].

The absorption of light by metal in the waveguide leads to heat generation and the resistive loss (heat power volume density) q is related to the metal loss and the electric field distribution in the waveguide by [13]:

$$q = \frac{1}{-}$$

of metal (4tn3 electric field.

B. Thermal Simulation

In reality, the heat power volume density decreases as light

(3-D) simulation is preferable. The temperature change along

analysis. On the one hand, as the light propagates along the waveguide, the power is exponentially attenuated and the resistive loss scales down correspondingly. On the other hand, the heat also conducts in the propagation direction. Therefore, the temperature change along the propagation direction depends on the combined effect of these two factors. However, the 3-D simulation poses severe requirement on the time and the perfor-

cross-section plane (x–y plane) of the waveguide and neglect it in the z direction, which is still meaningful to unveil the lateral photothermal properties although it overestimates the temperature change. The steady temperature T profile can be obtained by solving the heat transfer equation:

$$\nabla \cdot (\ k\ \ T) = q \tag{3}$$

where k is thermal conductivity of the material. Their values at room temperature (T / 293.15 K4 are provided in Table I and their temperature-dependent properties are taken into consideration in simulation. The thermal conductivity will be reduced due to strong boundary scattering effect for a thin material film. In calculation, bulk values are used for simplicity. q, which is the source for the temperature rise in the waveguides, can be calculated from Eq. (2).

The simulation is performed based on the finite element method (Comsol Multiphysics). This method has been validated in Ref. [29] and also reported by several other groups [17], [30]. The simulation region is assumed to be 300 $\times$ 300 μm^2 and the PW is located in the center of this region. All the interior boundaries are assumed to be continuous. At the lower exterior boundary in the y direction, the temperature of the silica substrate is set to room temperature. At the upper exterior boundary in the y direction, a convective heat transfer coefficient of 20 W/(m^2·K) is assumed to account for the convective heat flux to the air environment. At the boundaries of $x = 150$ μm and $x = -150$ μm, the heat flux in the horizontal direction is set to zero, which is equivalent to periodic condition. Therefore, the waveguide is no longer treated as a standalone object, but as an array with a lattice constant of 300 μm in the x direction. Since the lattice constant is large enough, this assumption is valid for describing the practical boundary.

III. Optical Properties of the PWs

Through mode simulations, the electric field and resistive loss for the plasmonic modes supported by the five PWs (the metal is Au) are obtained and their profiles are provided in Fig. 2.

1) *Nanowire PW:* the electric field symmetrically surrounds the gold nanowire. The heat power volume density falls off from the nanowire periphery to the center since the penetration depth of electric field into gold is around 25 nm.
2) *Slot PW:* the electric field is mainly confined to the air slot. Therefore, the heat source mostly locates on the gold edge near the slot.
3) *Channel PW:* the electric field concentrates at the bottom of the V-shaped groove in the metal film. Therefore, the maximum resistive loss occurs in the gold near the groove bottom.
4) *Dielectric-loaded PW:* the electric field mainly focuses in the dielectric above the Au/PMMA interface. Compared with conventional photonic mode, the gold film acts as a mirror intersecting the PMMA ridge, thereby reducing the mode area significantly. The heat source mainly locates in the 25 nm gold layer below the PMMA ridge.
5) *Hybrid PW:* the electric field is strongly confined within the low-permittivity SiO_2 gap sandwiched between a gold cap and a high-permittivity Si ridge. The heat source locates mostly in the 50 nm-thick gold cap.

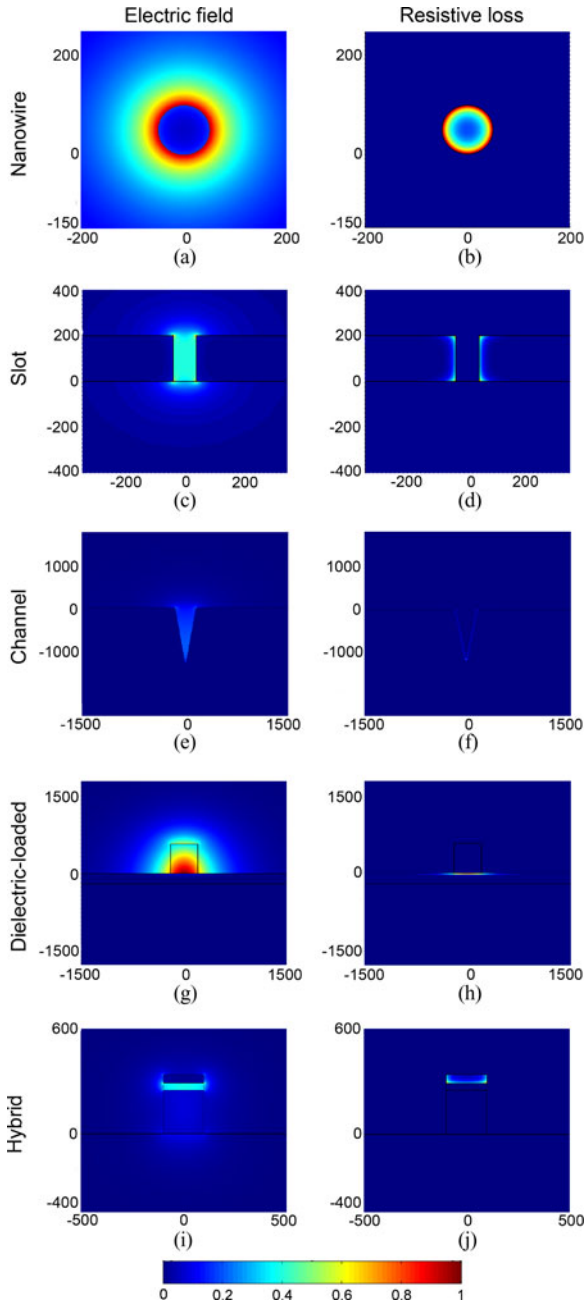

Fig. 2. Normalized electric field and resistive loss for the five Au PWs. (a) and (b) Nanowire PW with $r = 50$ nm, (c) and (d) slot PW with $W_2 = 80$ nm and $H_2 = 200$ nm, (e) and (f) channel PW with $W_3 = 320$ nm and $H_3 = 1200$ nm, (g) and (h) dielectric-loaded PW with $W_4 = 400$ nm and $H_4 = 600$ nm, and (i) and (j) hybrid PW with $W_5 = 200$ nm and $H_5 = 250$ nm.

IV. Thermal Properties of the PWs

The resistive loss, which acts as an effective heat source, results in a temperature rise in the waveguide. This section describes the thermal properties of the PWs, including spatial thermal properties and maximum temperature rise versus waveguide geometries and metal materials. The input CW light power is assumed to be 1 mW except specified. The considered power (1 mW) is compatible with those involved in practical situations. For a pulsed light, a transient response needs to be considered and the melting of metal at a high peak power can be expected.

A. Spatial Thermal Properties

Fig. 3 provides the temperature field profiles for the five Au PWs. The results show that the accumulated temperature for the nanowire PW, the slot PW, the channel PW, the dielectric-loaded PW, and the hybrid PW increases by 278.52 K, 113.23 K, 27.48 K, 18.93 K and 252.04 K, respectively. The nanowire PW and the hybrid PW have significant temperature rises. For these two PWs, the heat source areas are merely 0.0079 μm^2 and 0.01 μm^2, respectively. Besides, these two particular

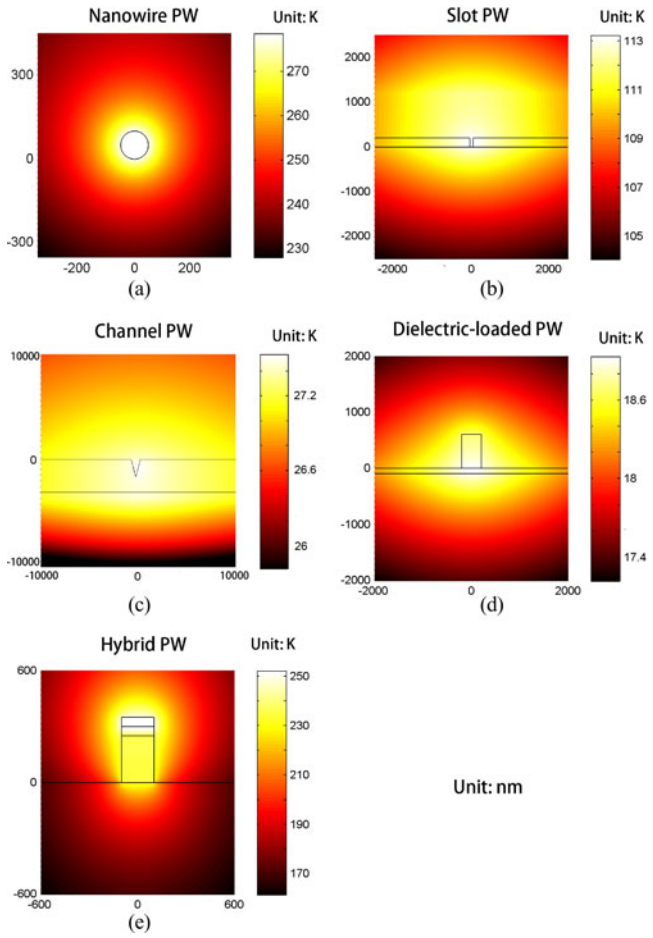

Fig. 3. Temperature rise profiles for the five Au PWs. The geometrical parameters are the same as those shown in Fig. 2.

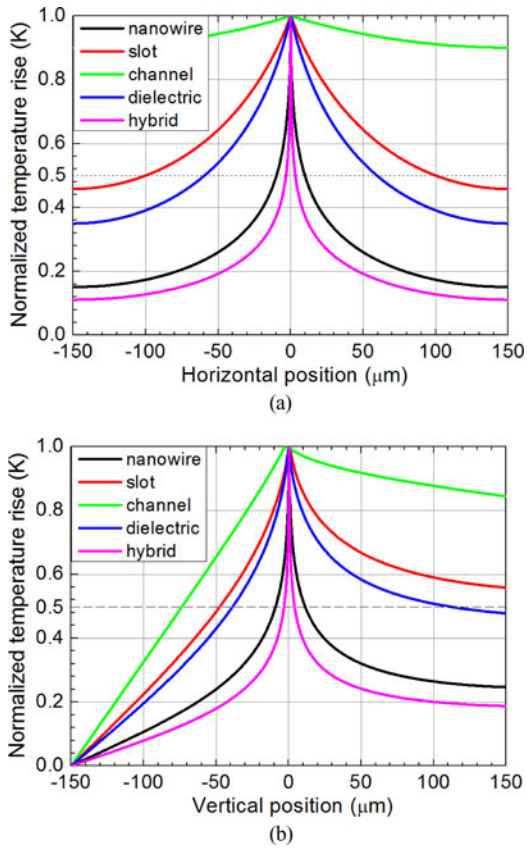

Fig. 4. Spatial distribution of temperature rise in (a) the horizontal (x-direction) and (b) vertical direction (y-direction) for the five Au PWs. The temperature rises are normalized to the maxima. The geometrical parameters are the same as those shown in Fig. 2.

waveguides are fully surrounded by dielectrics with low thermal conductivities. The generated heat, which cannot be readily exhausted out of the source, accumulates in these tiny areas and thus leads to significant temperature rises. For the channel PW and the dielectric-loaded PW, there are gold films below the air channel and the dielectric ridge, respectively. These gold films serve as efficient channels for exhausting the heat out of the heat sources, thereby alleviating the maximum temperature rise ($\Delta T_{\max}$) to a great extent. When the temporal thermal behavior is considered, the rising time is on the scale of $\sim$ 0.1 ms and $\sim$ 0.01 ms for the nanowire and hybrid PWs, respectively. For the slot PW, the channel PW, and the dielectric PW, the rising time is on the scale of $\sim$1 ms.

The strong photothermal effect can cause thermal crosstalk since the heat can be conducted from one waveguide to the adjacent waveguides. This thereby has a side effect on the integration density when the PWs are exploited for optical interconnect. In order to gain a deeper understanding, we further analyze the spatial temperature distributions for the five PWs, which are shown in Fig. 4. For the nanowire PW and the hybrid PW, the temperature rise in the horizontal direction (x-direction) decreases far more quickly compared with the other three PWs. The temperature gradient is inversely proportional to the thermal conductivity. The heat sources for the nanowire PW and the hybrid PW are surrounded by dielectrics with low thermal conductivities, consequently resulting in large temperature gradients. For the hybrid PW, the temperature rise at 3.25 μm away from the waveguide can still be half of the maximum temperature rise. For dielectric-loaded PW, this value rises to 60 μm. These values are at least one order of magnitude larger than the feature sizes of PWs; therefore, to alleviate the thermal crosstalk, the two PWs have to be positioned apart with a distance much larger than the waveguides feature sizes. The maximum integration density for PWs will ultimately be limited by their thermal feature length rather than the optical feature size, just as the problem that is confronted by electronic devices.

B. Maximum Temperature Versus Waveguide Geometries, Metal Materials

We also analyze the dependence of effective propagation length and maximum temperature rise on waveguide width (or nanowire radius) and metal materials for the five PWs and the results are shown in Fig. 5.

1) *Propagation length:* For each PW of different metals, Cu waveguides exhibit the shortest propagation length, followed by Au waveguides and Ag waveguides. Al waveguides show the longest propagation length. This can be

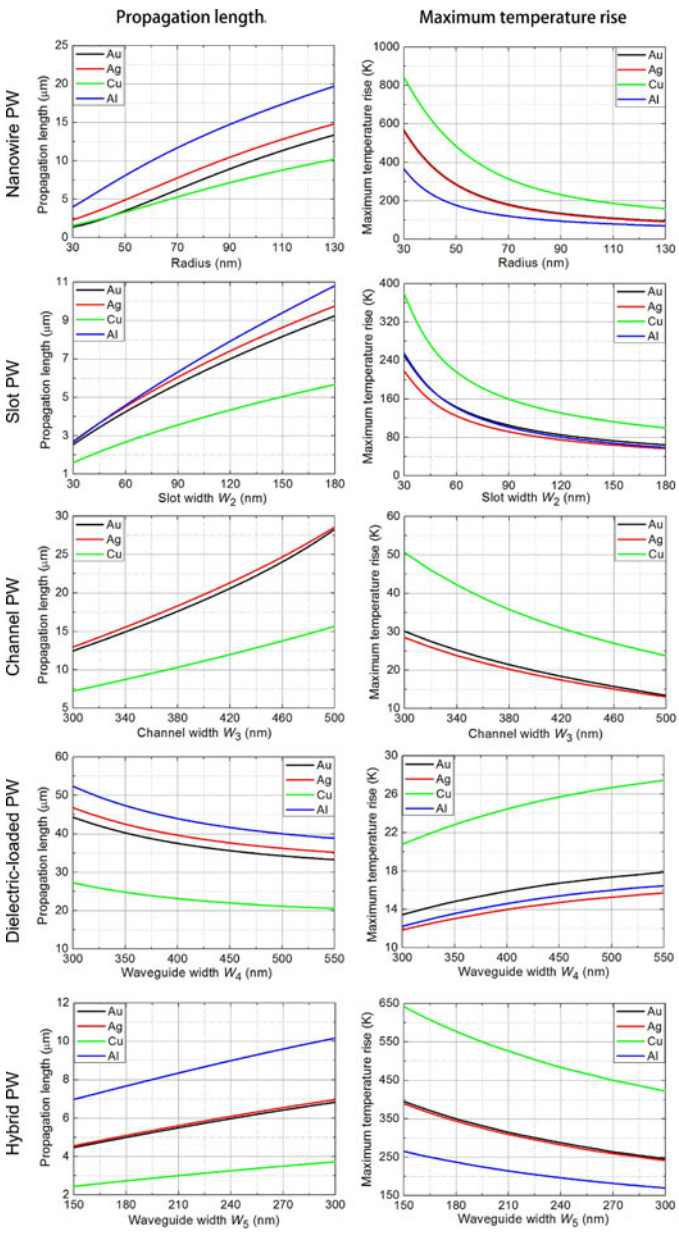

Fig. 5. Dependence of (left) effective propagation length and (right) maximum temperature rise on nanowire radius/waveguide width. The geometrical parameters are the same as those shown in Fig. 2 except the nanowire radius/waveguide width.

explained in terms of the metal permittivity. The plasmon propagation loss between the metal/dielectric interface is proportional to $\varepsilon_m''/{\varepsilon_m}'^2$. From the permittivity presented in Table I, we can see that Cu has the largest propagation loss.

2) *Maximum temperature rise:* The maximum temperature rise is not only related to the resistive loss, but also to the thermal conductivity. i) For the nanowire PW and the hybrid PW, the heat sources are surrounded by dielectrics with low thermal conductivities and the resistive loss contributes predominantly to the temperature rise. Therefore, Cu waveguide exhibits the largest temperature rise while the Al waveguide the smallest temperature rise. ii) For the slot PW, the channel PW and the dielectric-loaded PW, the metal layers are the main channels for exhausting the heat and thus the metal thermal conductivity plays a substantial role in the heat accumulation. For these three particular PWs, the temperature rise can be approximately proportional to $\varepsilon_m''/k\varepsilon_m'^2$. From the permittivity and thermal conductivity demonstrated in Table I, we can see that Cu has the largest $\varepsilon_m''/k\varepsilon_m'^2$, followed by Au, Al, and Ag. Therefore, the Cu waveguide exhibits the largest temperature rise and the Ag waveguide the smallest temperature rise.

V. Conclusion

The photothermal properties in five kinds of typical PWs for optical interconnect are considered in this paper, including nanowire PWs, slot PWs, channel PWs, dielectric-loaded PWs and hybrid PWs. For the nanowire PWs and the hybrid PWs, where the heat sources are fully surrounded by dielectrics, significant temperature rises can be expected. While for the slot PWs, the channel PWs, and the dielectric-loaded PWs, where the metal layers below serve as efficient heat exhaustion channels, smaller temperature rises can be expected compared with the nanowire PW and the hybrid PW. As to the spatial thermal distribution, the thermal feature sizes for all the PWs are well larger than their optical counterparts. Therefore, the maximum integration density for PWs will be limited by their thermal feature sizes even though the PWs can confine the light beyond the diffraction limit.

When different metals are adopted, Cu waveguide exhibits the largest temperature rise while the Al waveguide the smallest temperature rise for the nanowire PW and the hybrid PW, where the resistive loss contributes predominantly to the temperature rise. The Cu waveguide shows the largest temperature rise and the Ag waveguide the smallest temperature rise for the slot PW, the channel PW, and the dielectric-loaded PW, where the metal thermal conductivity plays a substantial role in the heat accumulation.

To reduce the heating, plasmonic materials with low losses should be used since they could fundamentally reduce the resistive loss forming the heat sources. These findings presented in this paper unveil the physical properties of PWs from the photothermal perspective and provide insights into some of the underlying factors influencing the adoption of PWs for optical interconnect.

References

[1] D. K. Gramotnev and S. I. Bozhevolnyi, "Plasmonics beyond the diffraction limit," *Nat. Photon*, vol. 4, no. 2, pp. 83–91, Jan. 2010.

[2] R. Zia, J. A. Schuller, A. Chandran, and M. L. Brongersma, "Plasmonics: The next chip-scale technology," *Mater. Today*, vol. 9, no. 7–8, pp. 20–27, Jul. 2006.

[3] E. Ozbay, "Plasmonics: Merging photonics and electronics at nanoscale dimensions," *Science*, vol. 311, no. 5758, pp. 189–193, Jan. 2006.

[4] M. L. Brongersma, R. Zia, and J. A. Schuller, "Plasmonics—The missing link between nanoelectronics and microphotonics," *Appl. Phys. A.*, vol. 89, no. 2, pp. 221–223, Nov. 2007.

[5] Z. P. Li, K. Bao, Y. R. Fang, Y. Z. Huang, P. Nordlander, and H. X. Xu, "Correlation between incident and emission polarization in nanowire

surface plasmon waveguides," *Nano Lett*, vol. 10, no. 5, pp. 1831–1835, Apr. 2010.
[6] G. Veronis and S. Fan, "Guided subwavelength plasmonic mode supported by a slot in a thin metal film," *Opt. Lett.*, vol. 30, no. 24, pp. 3359–3361, Dec. 2005.
[7] D. F. P. Pile, T. Ogawa, D. K. Gramotnev, Y. Matsuzaki, K. C. Vernon, K. Yamaguchi, T. Okamoto, M. Haraguchi, and M. Fukui, "Two-dimensionally localized modes of a nanoscale gap plasmon waveguide," *Appl. Phys. Lett.*, vol. 87, no. 26, p. 261114, Dec. 2005.
[8] L. Chen, J. Shakya, and M. Lipson, "Subwavelength confinement in an integrated metal slot waveguide on silicon," *Opt. Lett.*, vol. 31, no. 14, pp. 2133–2135, Jul. 2006.
[9] S. I. Bozhevolnyi, V. S. Volkov, E. Devaux, J. Y. Laluet, and T. W. Ebbesen, "Channel plasmon subwavelength waveguide components including interferometers and ring resonators," *Nature*, vol. 440, no. 7083, pp. 508–511, Mar. 2006.
[10] C. Reinhardt, S. Passinger, B. N. Chichkov, C. Marquart, I. P. Radko, and S. I. Bozhevolnyi, "Laser-fabricated dielectric optical components for surface plasmon polaritons," *Opt. Lett.*, vol. 31, no. 9, pp. 1307–1309, Jan. 2006.
[11] R. F. Oulton, V. J. Sorger, D. A. Genov, D. F. P. Pile, and X. Zhang, "A hybrid plasmonic waveguide for subwavelength confinement and long-range propagation," *Nat. Photon*, vol. 2, no. 8, pp. 496–500, Aug. 2008.
[12] O. Govorov and H. H. Richardson, "Generating heat with metal nanoparticles," *Nano Today*, vol. 1, no. 2, pp. 30–38, Feb. 2007.
[13] G. Baffou, R. Quidant, and F. J. García de Abajo, "Nanoscale control of optical heating in complex plasmonic systems," *ACS Nano*, vol. 4, no. 2, pp. 709–716, Jan. 2010.
[14] A. M. Gobin, M. H. Lee, N. J. Halas, W. D. James, R. A. Drezek, and J. L. West, "Near-infrared resonant nanoshells for combined optical imaging and photothermal cancer therapy," *Nano Lett*, vol. 7, no. 7, pp. 1929–1934, Jun. 2007.
[15] X. Chen, Y. Chen, M. Yan, and M. Qiu, "Nanosecond photothermal effects in plasmonic nanostructures," *ACS Nano*, vol. 6, no. 3, pp. 2550–2557, Feb. 2012.
[16] P. Zijlstra, J. W. M. Chon, and M. Gu, "Five-dimensional optical recording mediated by surface plasmons in gold nano-rods," *Nature*, vol. 459, no. 7245, pp. 410–413, May 2009.
[17] J. S. Donner, G. Baffou, D. McCloskey, and R. Quidant, "Plasmon-assisted optofluidics," *ACS Nano*, vol. 5, no. 7, pp. 5457–5462, Jun. 2011.
[18] B. J. Roxworthy and K. C. Toussaint, "Plasmonic nanotweezers: Strong influence of adhesion layer and nanostructure orientation on trapping performance," *Opt. Exp.*, vol. 20, no. 9, pp. 9591–9603, Apr. 2012.
[19] J. C. Weeber, K. Hassan, L. Saviot, A. Dereux, C. Boissière, O. Durupthy, C. Chaneac, E. Burov, and A. Pastouret, "Efficient photo-thermal activation of gold nanoparticle-doped polymer plasmonic switches," *Opt. Exp.*, vol. 20, no. 25, pp. 27636–27649, Nov. 2012.
[20] W. Zhang, Q. Li, and M. Qiu, "A plasmon ruler based on nanoscale photothermal effect," *Opt. Exp.*, vol. 21, no. 1, pp. 172–181, Jan. 2013.
[21] G. Gonzalez de la Cruz and Y. G. Gurevich, "Heat transport across metal–semiconductor (dielectric) structure under steady," *J. Heat Mass Transfer*, vol. 55, no. 15, pp. 4264–4268, Jul. 2012.
[22] O. Govorov and H. H. Richardson, "Generating heat with metal nanoparticles," *Nano Today*, vol. 1, no. 2, pp. 30–38, Feb. 2007.
[23] V. P. Zhdanov, I. Zoric, and B. Kasemo, "Plasmonics: Heat transfer between metal nanoparticles and supporting nanolayers," *Physica E*, vol. 46, pp. 113–118, Sep. 2012.
[24] G. Baffou and R. Quidant, "Thermo-plasmonics: Using metallic nanostructures as nano-sources of heat," *Laser Photon. Rev.*, vol. 7, no. 2, pp. 171–187, Mar. 2013.
[25] J. Zhu, Z. Sun, J. J. Li, and J. W. Zhao, "Local temperature pattern in plasmonic gold nanoshell: Tuning the heat generation," *Eur. Phys. J. B*, vol. 78, no. 3, pp. 311–314, Dec. 2010.
[26] E. D. Palik, *Handbook of Optical Constants of Solids*. New York, NY, USA: Academic, 1997.
[27] A. D. Rakić, "Algorithm for the determination of intrinsic optical constants of metal films: application to aluminum," *Appl. Opt.*, vol. 34, no. 22, pp. 4755–4767, Aug. 1995.
[28] [Online]. Available: http://www.mit.edu/∼6.777/matprops/pmma.htm
[29] X. Chen, Y. Chen, M. Yan, and M. Qiu, "Nanosecond photothermal effects in plasmonic nanostructures," *ACS Nano*, vol. 6, no. 3, pp. 2550–2557, Feb. 2012.
[30] S. Cheong, S. Krishnan, and S. Cho, "Modeling of plasmonic heating from individual gold nanoshells for near-infrared laser-induced thermal therapy," *Med. Phys.*, vol. 36, no. 10, pp. 4664–4671, Sep. 2009.

Qiang Li (M'13) received the B.S. and M.S. degrees from Harbin Institute of Technology, Heilongjiang, China, and the Ph.D. degree from Royal Institute of Technology, Stockholm, Sweden, in 2005, 2007 and 2011, respectively. He is currently a Lecturer in the Department of Optical Engineering, Zhejiang University. His research interest mainly focuses on nanophotonics.

Weichun Zhang received the B.S. degree from China Jiliang University, Hangzhou, China, in 2011. He is currently working toward the Master's degree in Zhejiang University. His research interest includes the area of plasmonics.

Hang Zhao is currently working toward the Bachelor's degree in Zhejiang University. His research interest includes the area of plasmonics.

Min Qiu (M'99–SM'13) received the B.Sc. and Ph.D. degrees in condense matter physics from Zhejiang University, Hangzhou, China, in 1995 and 1999, respectively, and the Ph.D. degree in electromagnetic theory from the Royal Institute of Technology (KTH), Stockholm, Sweden, in 2001.

In 2001, he joined KTH as an Assistant Professor. He became an Associate Professor in 2005, and a Full Professor of Photonics in 2009. He is now a Professor in the Department of Optical Engineering, Zhejiang University. He is an author or coauthor of more than 150 international refereed journal papers, and more than 100 conference contributions. He received the Individual Grant of "Future Research Leader" (INGVAR) from the Swedish Foundation for Strategic Research (SSF) in 2004. His research focuses mostly on nanophotonics, including optical metamaterials, photonic crystals, plasmonics, silicon photonics, and integrated optical circuits.